



Heat transfer effects on the oscillatory MHD flow in a porous channel with two immiscible fluids

Medisetty Padma Devi^a, Suripeddi Srinivas^b

Department of Mathematics, VIT-AP University,
Inavolu-522 237, Near Vijayawada, Andhra Pradesh, India
padmadevimesetti@gmail.com; srinusuripeddi@hotmail.com

Received: July 12, 2022 / Revised: January 23, 2023 / Published online: February 22, 2023

Abstract. The MHD oscillatory flow of two immiscible, viscous liquids in a porous channel with heat transfer is the subject of this investigation. The two liquid layers with different viscosities flow in both regions. The analytical expressions for velocity and temperature distribution have been derived by solving the governing flow equations using the regular perturbation method. The effects of various parameters on the velocity, temperature, and Nusselt number have been shown graphically, and numerical values of skin friction and flow rate are presented in tabular form and discussed. According to our analysis, the mass flux reduces as the magnetic field strength rises. While the temperature of the liquid enhances with an increase in the Eckert number and the Prandtl number, the temperature distribution rises with a decrease in the thermal conductivity ratio. To validate the results, the analytical solutions are compared with the fourth-order numerical Runge–Kutta method coupled with the shooting approach, and the results are found to be in excellent agreement.

Keywords: oscillatory MHD flow, permeable walls, Rosseland approximation, Hartmann number, cross-flow Reynolds number.

1 Introduction

Recent research on the flows of immiscible liquids in porous space reflects the phenomenon's growing technical value in a variety of disciplines. Soil mechanics, groundwater hydrology, crude oil purification, water-to-oil mixtures in packed rocks, chemical engineering, etc. are fields where immiscible fluid flows occur [2, 4, 8, 12, 15–18, 20, 24, 27, 31, 32]. Packham and Shail [16] investigated the problem of two immiscible steady cocurrent viscous liquid flows in a pipe. Their findings indicate that if the cross-section of the duct is symmetric with respect to the interface, the velocity distribution can be expressed in terms of two different pipe-flow solutions. One corresponds to a single layer flow occupying the full pipe, while the other corresponds to a comparable flow in a pipe whose cross-section coincides with the space filled by a single liquid in two-phase motion. A solution

for the imbibition phenomenon caused by relative wettability of flowing liquid in double-phase flow through porous media has been explored by Mishra and Verma [15]. The influence of peripheral-layer viscosity on time-averaged flux and mechanical efficiency was investigated. Trapping zone's development and growth in the core and peripheral layers are explained by Pouliquen et al. [18]. Under the assumptions of long-wavelength and low Reynolds number approximations, Ramachandra and Usha [20] investigated the peristaltic motion of two immiscible viscous liquids in a circular tube in copumping and pumping ranges. Umavathi et al. [27] explored the Poiseuille–Couette flow of two immiscible liquids between inclined parallel plates assuming that one of the liquids is electrically conducting, while the other liquid and channel walls are electrically insulating. In their model, the viscous and Ohmic dissipation terms are accounted for in the energy equation. The starting flow due to a sudden pressure gradient in a channel containing two layers of different liquids is investigated by Wang [31]. Ansari and Deo [2] examined the flow of viscous liquids of various viscosities in the presence of a constant pressure gradient with two distinct layers of equal width. With the assumption that the bottom layer's fluid viscosity is greater than the top layer's, analytical solutions for the velocity distribution and flow rate are produced. The laminar flow of two viscous, incompressible, electrically conducting, and heat-generating or -absorbing immiscible fluids in an indefinitely long, impermeable parallel-plate channel filled with a uniform porous media was investigated by Chamkha [8]. The MHD mixed convection flow in a vertical channel with two regions between flat walls is examined by Petrovic et al. [17]. It is assumed that both regions are filled with porous media of different/equal permeability. Region I contains the nanofluid whose base fluid is immiscible with the pure fluid flowing through region II. Very recently, Bitla and Sitotaw [4] studied the combined influences of slip and inclined uniform magnetic field on immiscible liquids (couple stress fluid and Jeffrey liquid) flow in a porous channel. Most recently, Yadav et al. [32] analyzed the influences of oriented magnetic fields and thermal radiation on the entropy generation of two immiscible electrically conducting micropolar and Newtonian liquids in a rectangular enclosure.

Pulsating flow problems in a channel or tube have captured a lot of attention recently because of their potential applications in engineering and biological systems (see [13, 14, 19, 21, 22, 30, 33]). Radhakrishnamacharya and Maiti [19] investigated thermal effects of Newtonian viscous flow in a porous channel with oscillatory pressure gradient. Mandal [14] examined a theoretical study to explore some of the significant characteristics of nonlinear blood flow through a constricted flexible artery under the influence of a pulsating pressure gradient. The flowing blood is characterised by a two-liquid model consisting of a core region of suspension of all erythrocytes assumed to be non-Newtonian and a peripheral layer of plasma as a Newtonian liquid. The fluid is injected from the lower wall, and suction takes place from the upper wall of the channel. Subhashis Ray et al. [21] performed numerical simulations to understand the development length of sinusoidally pulsating laminar pipe flows in moderate and high Reynolds number regimes. Vijayalakshmi and Srinivas [30] analyzed the thermal radiation effect on MHD pulsating nanofluid in a porous channel considering base fluid as water with nanoparticles of silver (Ag), copper (Cu), alumina (Al_2O_3), and titanium dioxide (TiO_2). The effective thermal

conductivity and viscosity of the nanofluid are calculated using the Maxwell–Garnetts and Brinkman models. The pulsating flow of Eyring–Powell nanofluid in a porous channel with a magnetic field was studied by Bharatkumar and Srinivas [13]. Blood was used as the non-Newtonian base fluid, and gold and aluminum oxide were used as nanoparticles. The pulsating Casson fluid slip flow in a vertical porous space with heat mass transfer effects, assuming the liquid is injected into the channel from the left and then withdrawn at the same velocity from the opposite wall, is reported recently by Srinivas et al. [22].

Flows in porous space are of great interest due to their prevalence in nature. Such flows have a variety of scientific and engineering applications including studying underground water resources and seepage of water in river beds in agriculture engineering, filtration and purification processes in chemical engineering, and the movement of natural gases, oil, and water through reservoirs in petroleum technology [1, 11, 23, 32]. Multiphase flow with heat transport is being studied in a number of fields. MHD power generation, the petroleum industry, and magneto-fluid dynamics are all important uses. A wide number of important practical problems of interest are unsteady. Further, despite a large number of oscillatory flow investigations in different flow configurations (see [6–9, 11] and references therein), only a few investigations on immiscible flows with oscillatory pressure gradient have been documented. Umavathi et al. [25] explored the heat transfer effect on the time-dependent flow of two immiscible liquids in a channel with transpiring walls that oscillate at a time-dependent normal velocity. Umavathi et al. [28] reported the time dependent flow of MHD two immiscible liquids in a channel with heat transfer. It is assumed that one of the fluids and the channel walls are electrical insulated, and the other fluid is considered to have electrical conductivity. Thermal effect on the time-dependent flow in a composite channel with two parallel permeable plates along with a fluid-saturated porous layer filling half of the distance between them and a clear viscous liquid filling the other half was investigated by Umavathi et al. [26]. In a recent work, Tiwari and Chauhan [23] explored the oscillatory blood flow with porous boundary in a tube accounting for the effect of hematocrit-dependent viscosity. Most recently, Padma Devi and Srinivas [10] studied the influence of thermal radiation effects on pulsating MHD flow of two immiscible liquids in a channel filled with porous space.

Despite a significant amount of research on the topic of oscillatory flows in channels and tubes, very few publications relevant to immiscible liquids with an oscillating pressure gradient have been reported in the literature. Motivated by the works of Umavathi et al. [25, 26] and Attia et al. [3] and keeping in view of the practical importance of the oscillatory MHD flow of immiscible liquids in a channel, an attempt has been made to present a mathematical model. Assuming that the channel is filled with a porous media, the problem of thermal effects of the pulsating MHD flow of two immiscible liquids in a horizontal channel with transpiring walls, accounting for the thermal radiation effect, has been investigated in our present study. Closed-form expressions have been obtained for the dimensionless velocity and temperature distributions. The effects of a number of emergent parameters on temperature and velocity distributions have been graphically depicted, and numerical values for flow rate and stress distribution have been provided in a tabular form and quantitatively discussed.

2 Mathematical formulation

Figure 1 shows the geometry under consideration containing two regions I and II with porous medium permeabilities of K_1 and K_2 , respectively. It is considered that regions I is $-h \leq y \leq 0$, and $0 \leq y \leq h$ represents region II. Region I with a conducting viscous liquid of density ρ_1 , viscosity μ_1 and the other region is filled with a liquid of density $\rho_2 (< \rho_1)$ and viscosity μ_2 . The immiscible fluids are supposed to be incompressible, and the flow is time dependent with an oscillatory pressure gradient driving it. It may be noted that conducting liquids are immiscible with permeable channel walls at rest. The temperature of the lower and upper channel walls are T_{w1} and T_{w2} , respectively. The induced magnetic field is neglected as the Hall effect of magnetohydrodynamics is considered to be insignificant due to the low magnetic Reynolds number [6,9,29]. Further, to simplify the governing equation the following assumptions [28] are used: (a) in the porous medium the flow is laminar and incompressible; (b) the porous medium isotropic and homogenous in both regions; (c) the fluid and solid phases in the porous medium are assumed to have constant thermophysical properties; (d) the porous media non-Darcian inertial parameter, which represents the additional pressure loss due to interpore mixing present at high velocities, can be overlooked for sluggish flow in the porous medium [5,7].

Region I:

$$\rho_1 \left(\frac{\partial u_1}{\partial t} + v_1 \frac{\partial u_1}{\partial y} \right) = -\frac{\partial p}{\partial x} + \mu_1 \frac{\partial^2 u_1}{\partial y^2} - \sigma_1 B_0^2 u_1 - \frac{\mu_1 u_1}{K_1}, \tag{1}$$

$$\rho_1 c_p \left(\frac{\partial T_1}{\partial t} + v_1 \frac{\partial T_1}{\partial y} \right) = K_1 \frac{\partial^2 T_1}{\partial y^2} + \mu_1 \left(\frac{\partial u_1}{\partial y} \right)^2 - \frac{\partial q_r}{\partial y}. \tag{2}$$

Region II:

$$\rho_2 \left(\frac{\partial u_2}{\partial t} + v_2 \frac{\partial u_2}{\partial y} \right) = -\frac{\partial p}{\partial x} + \mu_2 \frac{\partial^2 u_2}{\partial y^2} - \sigma_2 B_0^2 u_2 - \frac{\mu_2 u_2}{K_2}, \tag{3}$$

$$\rho_2 c_p \left(\frac{\partial T_2}{\partial t} + v_2 \frac{\partial T_2}{\partial y} \right) = K_2 \frac{\partial^2 T_2}{\partial y^2} + \mu_2 \left(\frac{\partial u_2}{\partial y} \right)^2 - \frac{\partial q_r}{\partial y}, \tag{4}$$

where x -component velocity is u , y -component velocity is v , and fluid temperature is represented by T , ρ_1 and ρ_2 are the densities, C_p is the specific heat, k_1 and k_2 are the ratio of thermal conductivities, v_1 and v_2 are injection and suction at lower and upper walls of the channel. The subscripts 1 and 2 are for region I and region II, respectively. By invoking no-slip boundary conditions, velocity in the x -direction is zero at the walls of the channel. Further, there is a continuity of the velocity, shear-rate, temperature at the interface between the two liquid layers. B_0 is the magnetic induction of the uniform magnetic field. σ_1 and σ_2 are the electrical conductivity of the fluid. q_r^* represents the radiative heat flux. The radiative heat flux q_r^* , using the Rosseland approximation, is $q_r^* = -(4\sigma^*/(3k^*))\partial T^{*4}/\partial y^*$. Here $\sigma^* = (5.6697 \times 10^{-8} \text{ Wm}^{-2}\text{K}^{-4})$ and k^* represent the Stefan-Boltzmann constant and Rosseland mean absorption coefficient, respectively. Expressing T^{*4} as a linear function of T , under the assumption that within the liquid the

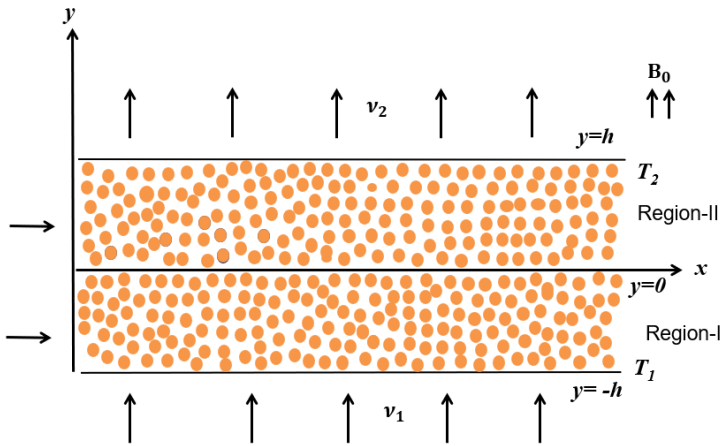


Figure 1. Sketch of the model.

temperature variations are small [30], we get

$$T^{*4} \cong 4T_1^3 T^* - 3T_1^4.$$

The fluid flow is subjected to the following conditions [25, 26, 28]:

$$\begin{aligned} u_1 &= 0, & T_1^* &= T_1 & \text{at } y &= -h, \\ u_2 &= 0, & T_2^* &= T_2 & \text{at } y &= h, \\ u_1 &= u_2, & T_1^* &= T_2^* & \text{at } y &= 0, \\ \mu_1 \frac{\partial u_1}{\partial y} &= \mu_2 \frac{\partial u_2}{\partial y}, & K_1 \frac{\partial T_1^*}{\partial y} &= K_2 \frac{\partial T_2^*}{\partial y} & \text{at } y &= 0, \end{aligned}$$

v_1 and v_2 representing injection and suction at lower and upper walls, respectively. Taking $v_1 = v_2 = v$ and

$$v = v_* (1 + \varepsilon_* B_* e^{i\omega t}),$$

where B_* is positive constant. ω denotes the frequency parameter, $\varepsilon_* = \text{const}$ and considered to be small. Periodically transpiration velocity varies with time about a nonzero constant mean v_* , and it is assumed here. The nondimensional quantities and the pressure gradient are

$$-\frac{\partial p}{\partial x} = \left(\frac{\partial p}{\partial x} \right)_s + \varepsilon_* \left(\frac{\partial p}{\partial x} \right)_o e^{i\omega t},$$

$P_s = (\partial p / \partial x)_s$, $P_o = (\partial p / \partial x)_o$ are the pulsations that are both steady and oscillating, respectively, and the frequency parameter is ω . $x = x^* / h$, $y = y^* / h$, $u_i^* = u_i / \bar{u}_1$, $u_{i1}^* = u_{i1} / \bar{u}_1$, $u_{i2}^* = u_{i2} / \bar{u}_1$, $t^* = tv / h^2$, $v^* = (h / \nu)v$, $R = v_* h / \nu$, $w^* = wh^2 / \nu$ (cross-flow Reynolds number), $K_i^* = K_i / h^2$, $\tau_i^* = \tau_i / (\rho u^2)$, $p^* = p / (\rho u^2)$, $M_1 = B_0 h \sqrt{\sigma_1 / \mu_1}$ (Hartmann number of region I), $M_2 = M_1 \sqrt{\beta / \gamma}$ (Hartmann number of region II), $\theta_i = (T_i^* - T_1) / (T_2 - T_1)$, $Pr = (\mu_1 / K_1) C_p$ (Prandtl number), $Rd = 4\sigma^* T_1^3 / (k^* K_1)$

(thermal radiation), $Ec = \bar{u}_1^2 / (C_p(T_2 - T_1))$ (Eckert number), $\alpha = \rho_1 / \rho_2$ (ratio of densities), $\beta = \mu_1 / \mu_2$ (ratio of viscosities), $\delta = k_2 / k_1$ (ratio of thermal conductivities), $\gamma = \sigma_1 / \sigma_2$ (ratio of electrical conductivities), $v = (\nu/h)v^* = \nu|v_*|$, $P = K_2 / K_1$ (ratio of permeabilities), $\alpha_1 = \beta / \alpha$.

Equations (1)–(4) are reduced when nondimensional quantities are introduced and the asterisks are removed: for region I,

$$\left(\frac{\partial u_1}{\partial t} + Rv \frac{\partial u_1}{\partial y} \right) = -\frac{\partial p}{\partial x} + \frac{\partial^2 u_1}{\partial y^2} - \left(M_1^2 + \frac{1}{K_1} \right) u_1, \tag{5}$$

$$\left(\frac{\partial \theta_1}{\partial t} + Rv \frac{\partial \theta_1}{\partial y} \right) = \left(\frac{1}{Pr} + \frac{4Rd}{3Pr} \right) \frac{\partial^2 \theta_1}{\partial y^2} + Ec \left(\frac{\partial u_1}{\partial y} \right)^2; \tag{6}$$

for region II,

$$\alpha_1 \left(\frac{\partial u_2}{\partial t} + Rv \frac{\partial u_2}{\partial y} \right) = -\beta \frac{\partial p}{\partial x} + \frac{\partial^2 u_2}{\partial y^2} - \left(M_2^2 + \frac{1}{K_2} \right) u_2, \tag{7}$$

$$\left(\frac{\partial \theta_2}{\partial t} + Rv \frac{\partial \theta_2}{\partial y} \right) = \left(\frac{\delta\alpha}{Pr} + \frac{4Rd\alpha}{3Pr} \right) \frac{\partial^2 \theta_2}{\partial y^2} + \frac{Ec}{\alpha_1} \left(\frac{\partial u_2}{\partial y} \right)^2. \tag{8}$$

The flow is subjected to the conditions

$$u_1 = 0, \quad \theta_1 = 0 \quad \text{at } y = -1, \tag{9}$$

$$u_2 = 0, \quad \theta_2 = 1 \quad \text{at } y = 1, \tag{10}$$

$$u_1 = u_2, \quad \theta_1 = \theta_2 \quad \text{at } y = 0, \tag{11}$$

$$\mu_1 \frac{\partial u_1}{\partial y} = \mu_2 \frac{\partial u_2}{\partial y}, \quad K_1 \frac{\partial \theta_1}{\partial y} = K_2 \frac{\partial \theta_2}{\partial y} \quad \text{at } y = 0. \tag{12}$$

For the velocity and temperature distributions in both regions, the governing equations (5)–(8) along with conditions (9)–(12) can be derived in the form [25, 28]

$$u_i = u_{i1} + \varepsilon_* u_{i2} e^{i\omega t}, \quad \theta_i = \theta_{i1} + \varepsilon_* \theta_{i2} e^{i\omega t}.$$

The steady and oscillatory flow governing equations are reduced to the following systems: steady flow

$$\frac{d^2 u_{11}}{dy^2} - R \frac{du_{11}}{dy} - \left(M_1^2 + \frac{1}{K_1} \right) u_{11} + P_s = 0, \tag{13}$$

$$\frac{d^2 u_{21}}{dy^2} - \alpha_1 R \frac{du_{21}}{dy} - \left(M_2^2 + \frac{1}{K_2} \right) u_{21} + \beta P_s = 0, \tag{14}$$

$$P_1 \frac{d^2 \theta_{11}}{dy^2} - R \frac{d\theta_{11}}{dy} + Ec \left(\frac{du_{11}}{dy} \right)^2 = 0, \tag{15}$$

$$P_{22} \frac{d^2 \theta_{21}}{dy^2} - R \frac{d\theta_{21}}{dy} + \frac{Ec}{\alpha_1} \left(\frac{du_{21}}{dy} \right)^2 = 0; \tag{16}$$

oscillatory flow

$$\frac{d^2 u_{12}}{dy^2} - R \frac{du_{12}}{dy} - \left(M_1^2 + \frac{1}{K_1} + i\omega \right) u_{12} - AR \frac{du_{11}}{dy} + P_0 = 0, \quad (17)$$

$$\frac{d^2 u_{22}}{dy^2} - \alpha_1 R \frac{du_{22}}{dy} - \left(M_2^2 + \frac{1}{K_2} + \alpha_1 i\omega \right) u_{22} - \alpha_1 AR \frac{du_{21}}{dy} + \beta P_0 = 0, \quad (18)$$

$$P_1 \frac{d^2 \theta_{12}}{dy^2} - R \frac{d\theta_{12}}{dy} - i\omega \theta_{12} - AR \frac{d\theta_{11}}{dy} + 2Ec \frac{du_{11}}{dy} \frac{du_{12}}{dy} = 0, \quad (19)$$

$$P_{22} \frac{d^2 \theta_{22}}{dy^2} - R \frac{d\theta_{22}}{dy} - i\omega \theta_{22} - AR \frac{d\theta_{21}}{dy} + 2 \frac{Ec}{\alpha_1} \frac{du_{21}}{dy} \frac{du_{22}}{dy} = 0. \quad (20)$$

The corresponding boundary conditions become as follows:

$$\begin{aligned} u_{11} = 0, \quad u_{12} = 0, \quad \theta_{11} = 0, \quad \theta_{12} = 0 & \quad \text{at } y = -1, \\ u_{21} = 0, \quad u_{22} = 0, \quad \theta_{21} = 1, \quad \theta_{22} = 0 & \quad \text{at } y = 1, \\ u_{11} = u_{21}, \quad u_{12} = u_{22}, \quad \theta_{11} = \theta_{21}, \quad \theta_{12} = \theta_{22} & \quad \text{at } y = 0, \\ \mu_1 \frac{\partial u_{11}}{\partial y} = \mu_2 \frac{\partial u_{21}}{\partial y}, \quad \mu_1 \frac{\partial u_{12}}{\partial y} = \mu_2 \frac{\partial u_{22}}{\partial y}, \\ K_1 \frac{\partial \theta_{11}}{\partial y} = K_2 \frac{\partial \theta_{21}}{\partial y}, \quad K_1 \frac{\partial \theta_{12}}{\partial y} = K_2 \frac{\partial \theta_{22}}{\partial y} & \quad \text{at } y = 0. \end{aligned}$$

3 Results of the problem

Steady flow described in equations (13)–(16) is given by

$$\begin{aligned} U_{11} &= C_1 e^{A_2 y} + C_2 e^{A_3 y} + A_{18}, \\ U_{21} &= C_5 e^{A_{10} y} + C_6 e^{A_{11} y} + A_{19}, \end{aligned}$$

$$\begin{aligned} \theta_{11} &= C_9 + C_{10} e^{RP_2 y} + P_4 e^{2A_2 y} + P_5 e^{2A_3 y} + L_6 e^{(A_2 + A_3) y}, \\ \theta_{21} &= C_{13} + C_{14} e^{RP_{23} y} + P_{25} e^{2A_{10} y} + P_{26} e^{2A_{11} y} + P_{27} e^{(A_{10} + A_{11}) y}. \end{aligned}$$

Oscillatory flow described in equations (17)–(20) is given by

$$\begin{aligned} U_{12} &= C_3 e^{A_5 y} + C_4 e^{A_6 y} + B_6 Re^{A_2 y} + A_7 Re^{A_3 y} + A_8, \\ U_{22} &= C_7 e^{A_{13} y} + C_8 e^{A_{14} y} + A_{15} Re^{A_{10} y} + A_{16} Re^{A_{11} y} + A_{17}, \end{aligned}$$

$$\begin{aligned} \theta_{12} &= C_{11} e^{P_{20} y} + C_{12} e^{P_{21} y} \\ &+ R^2 P_9 e^{RP_2 y} + RP_{10} e^{2A_2 y} + RP_{11} e^{2A_3 y} + RL_{11} e^{(A_2 + A_3) y} \\ &- P_{12} e^{(A_2 + A_5) y} - P_{13} e^{(A_2 + A_6) y} - RP_{14} e^{2A_2 y} - RP_{15} e^{(A_2 + A_3) y} \\ &- P_{16} e^{(A_3 + A_5) y} - P_{17} e^{(A_3 + A_6) y} - RP_{18} e^{(A_2 + A_3) y} - RP_{19} e^{2A_3 y}, \end{aligned}$$

$$\begin{aligned} \theta_{22} = & C_{15}e^{P_{31}y} + C_{16}e^{P_{32}y} \\ & + R^2P_{33}e^{RP_{23}y} + RP_{34}e^{2A_{10}y} + RP_{35}e^{2A_{11}y} + RP_{36}e^{(A_{10}+A_{11})y} \\ & - P_{37}e^{(A_{10}+A_{13})y} - P_{38}e^{(A_{10}+A_{14})y} - RP_{39}e^{2A_{10}y} - RP_{40}e^{(A_{10}+A_{11})y} \\ & - P_{41}e^{(A_{11}+A_{13})y} - L_{41}e^{(A_{11}+A_{14})y} - RL_{42}e^{(A_{10}+A_{11})y} - RP_{42}e^{2A_{11}y}, \end{aligned}$$

where

$$\begin{aligned} A_1 = M_1^2 + \frac{1}{K_1}, \quad A_2 = \frac{R + \sqrt{R^2 + 4A_1}}{2}, \quad A_3 = \frac{R - \sqrt{R^2 + 4A_1}}{2}, \\ A_4 = A_1 + \omega, \quad A_5 = \frac{R + \sqrt{R^2 + 4A_4}}{2}, \quad A_6 = \frac{R - \sqrt{R^2 + 4A_4}}{2}, \\ A_7 = \frac{B_*A_3C_2}{A_3^2 - RA_3 - A_4}, \quad A_8 = \frac{P_0}{A_4}, \quad A_9 = M_2^2 + \frac{1}{K_2}, \\ A_{10} = \frac{R\alpha_1 + \sqrt{R^2 + 4A_9}}{2}, \quad A_{11} = \frac{R\alpha_1 - \sqrt{R^2 + 4A_9}}{2}, \quad A_{12} = A_9 + \omega, \\ A_{13} = \frac{R\alpha_1 + \sqrt{R^2\alpha_1^2 + 4A_{12}}}{2}, \quad A_{14} = \frac{R\alpha_1 - \sqrt{R^2\alpha_1^2 + 4A_{12}}}{2}, \\ A_{15} = \frac{B_*\alpha_1C_5A_{10}}{A_{10}^2 - RA_{10} - A_{12}}, \quad A_{16} = \frac{B_*C_6\alpha_1A_{11}}{A_{11}^2 - RA_{11} - A_{12}}, \\ A_{17} = \frac{aP_0}{A_{12}}, \quad A_{18} = \frac{P_s}{A_1}, \quad A_{19} = \frac{\beta P_s}{A_9}. \end{aligned}$$

The Nusselt number is given by

$$Nu = \left(\frac{\partial \theta_1}{\partial y} \right)_{y=-1,1} + \varepsilon_* e^{\omega t} \left(\frac{\partial \theta_2}{\partial y} \right)_{y=-1,1}.$$

The skin friction at the walls can be obtained from

$$\tau_1 = \left(\frac{1}{R} \frac{\partial u_1}{\partial y} \right)_{y=-1,1}, \quad \tau_2 = \left(\frac{1}{\alpha R} \frac{\partial u_2}{\partial y} \right)_{y=-1,1}.$$

The flow rate in the regions I and II are as follows:

$$\begin{aligned} Q_1 = \int_{-1}^0 u_{11} dy + \varepsilon_* \left[\int_{-1}^0 u_{12} dy \right] e^{\omega t}, \\ Q_2 = \int_0^1 u_{21} dy + \varepsilon_* \left[\int_0^1 u_{22} dy \right] e^{\omega t}. \end{aligned}$$

4 Shearstress and massflux tables

Table 1. Variation of shearstress with viscosity at lower wall ($M_1 = 1, K_1 = 0.1$).

ωt	α				
	1	1.5	2	2.5	3
0	38.1987	17.249	17.7028	18.0116	18.234
$\pi/4$	210.8757	269.0525	305.1805	329.7975	347.6488
$\pi/2$	227.2824	290.7204	330.1327	356.9945	376.4771
π	227.0013	290.2134	329.4765	356.2308	375.6321

Table 2. Variation of shearstress with viscosity at upper wall ($M_1 = 1, K_1 = 0.1$).

ωt	α				
	1	1.5	2	2.5	3
0	18.3780	20.4232	21.6940	22.5522	23.1886
$\pi/4$	426.4041	631.0661	758.1629	844.7646	907.5654
$\pi/2$	458.2961	680.1070	817.9255	911.8631	979.9983
π	457.3337	678.8298	816.4572	910.2622	978.2991

Table 3. Variation of shearstress with permeability at lower wall ($M_1 = 1, \beta = 1$).

ωt	K_1				
	0.1	0.7	0.8	4	6
0	38.1987	28.8720	22.9679	17.8042	17.8659
$\pi/4$	154.9495	95.8267	158.0346	204.9536	241.6031
$\pi/2$	165.8972	102.4825	169.8677	220.6863	260.3490
π	165.8566	101.4846	168.4336	219.0335	258.5165

Table 4. Variation of shearstress with permeability at upper wall ($M_1 = 1, \beta = 1$).

ωt	K_1				
	0.1	0.7	0.8	4	6
0	18.3780	17.0156	16.9920	19.0424	18.9948
$\pi/4$	202.3083	172.4195	150.9035	134.6744	121.9970
$\pi/2$	216.1291	183.0788	159.3295	141.4503	127.5143
π	214.7513	181.7536	158.0796	140.3015	126.4929

Table 5. Variation of shearstress with M_1 at lower wall ($K_1 = 0.1, \beta = 1$).

ωt	M_1				
	0.1	0.5	1	1.5	2.5
0	36.8281	37.1755	38.1987	39.7201	16.8522
$\pi/4$	201.7956	204.0947	210.8757	220.9876	246.0617
$\pi/2$	217.3622	219.8743	227.2824	238.3330	265.7517
π	217.0461	219.5668	227.0013	238.0867	265.5622

Table 6. Variation of shearstress with M_1 at upper wall ($K_1 = 0.1, \beta = 1$).

ωt	M_1				
	0.1	0.5	1	1.5	2.5
0	17.3244	17.5617	18.3780	20.01447	21.4113
$\pi/4$	333.0033	354.5011	426.4041	563.2338	6.1833
$\pi/2$	357.9430	381.0420	458.2961	605.2922	6.4198
π	357.1798	380.2326	457.3337	604.0432	6.4130

Table 7. Variation of massflux with viscosity at both the walls ($M_1 = 1, K_1 = 0.1$).

ωt	α				
	1	1.5	2	2.5	3
0	0.5710	0.6543	0.7356	0.8163	0.8962
$\pi/4$	0.5337	0.6114	0.6874	0.7625	0.8372
$\pi/2$	0.5701	0.6532	0.7346	0.8150	0.8950
π	0.5674	0.6503	0.7314	0.8117	0.8914

Table 8. Variation of massflux with permeability at both the walls ($M_1 = 1, \beta = 1$).

ωt	K_1				
	0.1	0.7	0.8	4	6
0	0.5710	2.1761	2.3467	4.2283	4.5334
$\pi/4$	0.5337	2.0676	2.2329	4.0640	4.3608
$\pi/2$	0.5701	2.1292	2.2905	4.0362	4.3162
π	0.5674	2.0757	2.2322	3.9562	4.2361

Table 9. Variation of massflux with M_1 at both the walls ($K_1 = 0.1, \beta = 1$).

ωt	M_1				
	0.1	0.5	1	1.5	2.5
0	0.6123	0.6015	0.5710	0.5290	0.4393
$\pi/4$	0.5725	0.5625	0.5337	0.4941	0.4101
$\pi/2$	0.6111	0.6004	0.5701	0.5281	0.4388
π	0.6079	0.5973	0.5674	0.5259	0.4374

5 Discussion of results

The closed-form solutions obtained have been numerically evaluated for a wide range of parameters and the results are graphically (Figs. 2–6) and in the tabular form (Tables 1–9). Velocity distribution is displayed in Fig. 2 for the fixed values of $M_1 = 1, M_2 = 2, K_1 = 0.1, K_2 = 3, \omega = \pi/4, P_s = 2.5, P_o = 2, \alpha = 1, \beta = 1, \varepsilon_* = 0.1, R = 0.02, A = 0.1, t = 1$ on the velocity profiles. The influence of the ω on fluid velocity is depicted in Fig. 2(a). It is evident from the same that with a raise in the frequency the velocity of the fluid enhances. Figure 2(b) demonstrates the effect of the Hartmann number on the distribution of the velocity. A drag force will be developed, because of the magnetic field, which will act opposite to the flow. As a consequences, velocity of the fluid falls, as the magnetic field strength raises. The variation of velocity with R is illustrated in Fig. 2(c) and it reveals that the fluid velocity drops as the cross-flow Reynolds number raises. It is evident from Fig. 2(d) that the ratio of viscosity is raised, the viscosity of the fluid of the region I will be more, and thus fluid velocity in the lower region will be less when compared to upper region II, and a maximum velocity can be witnessed in the region II. The velocity distribution for various values of the permeability ratio parameter is shown in Fig. 2(e). A raise in the velocity can be observed with a rise in the permeability of the medium since barriers placed on the flow path reduce as P increases allowing for free flow thus increasing the velocity.

Temperature distribution is depicted in Fig. 3 taking $M_1 = 1, M_2 = 2, K_1 = 0.1, K_2 = 0.23, k_1 = 1, k_2 = 0.5, \omega = \pi/4, P_s = 2.5, P_o = 2, \alpha = 1, \beta = 1, \delta = 2, \gamma = 1,$

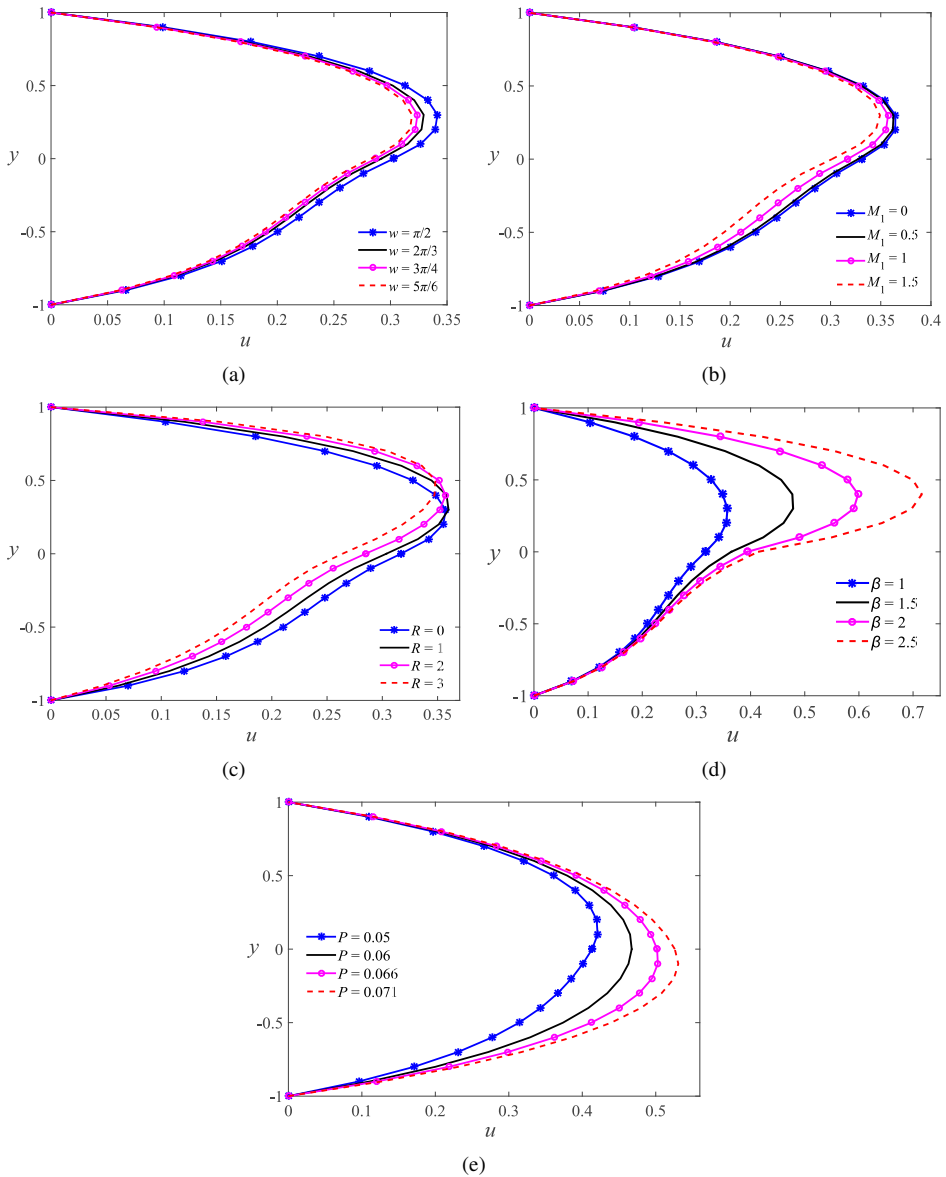


Figure 2. Velocity distributions: (a) influence of ω , (b) influence of M_1 , (c) influence of R , (d) influence of β , (e) influence of P .

$\varepsilon_* = 0.01$, $R = 0.02$ on the temperature profiles. Figure 3(a) reveals that as R raises, the fluid temperature falls. The thermal condition of the fluid in the channel tends to cool as the thermal conductivity ratio raises which is evident from Fig. 3(b). Figure 3(c) reveals that the temperature of the fluid falls with the increasing the value of radiation parameter.

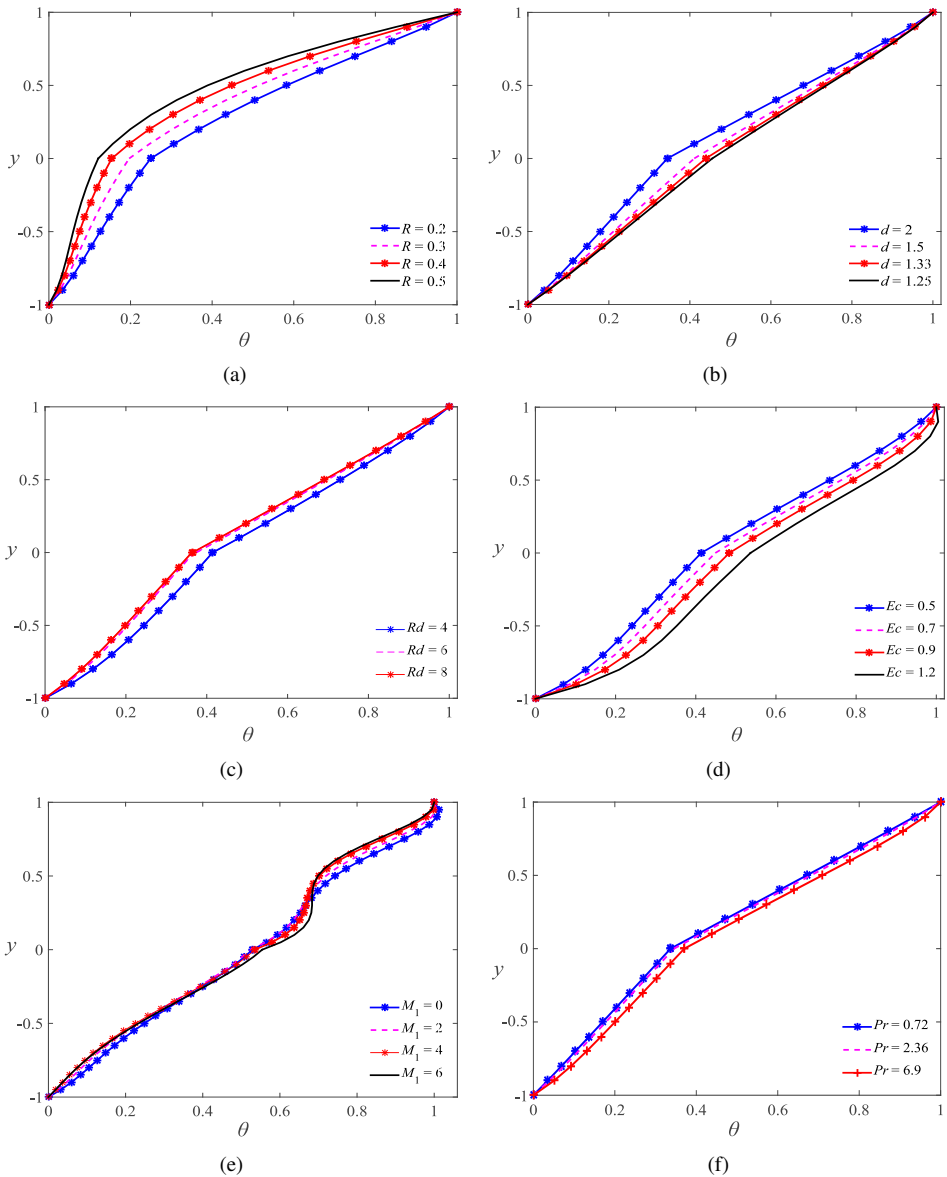


Figure 3. Temperature distributions: (a) influence of R , (b) influence of d , (c) influence of Rd , (d) influence of Ec , (e) influence of M_1 , (f) influence of Pr .

Since radiation has the effect of slowing down the rate of energy transfer to the fluid, which reduces the fluid's temperature, the results qualitatively correspond to expectations. Figures 3(d) and 3(f) are sketched to see the influence of Ec and Pr , respectively, on θ . The fluid temperature raises with Ec is true because the increase in kinetic energy within

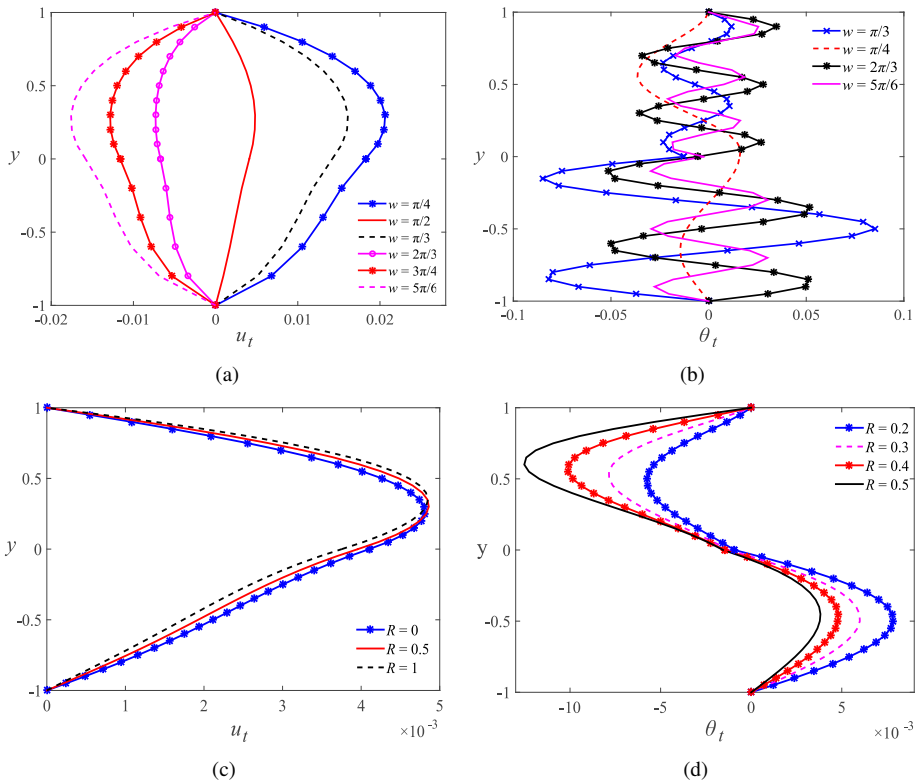


Figure 4. Variation of unsteady velocity and temperature profiles with (a)–(b) ω , (c)–(d) R .

the channel generates additional heat within the moving fluid. The values chosen for Pr are for the air ($Pr = 0.71$), carbondisulphide ($Pr = 2.36$) and water ($Pr = 6.9$). Figure 3(f) depicts the effect of the Prandtl number on the temperature distribution of the fluid. The increase in viscous diffusion that increases internal temperature due to the existence of viscous dissipation, resulting a rise in the temperature. The influence of M_1 on the distribution of temperature is illustrated in Fig. 3(e). It is clear that raise in M_1 causes the 0 temperature of the fluid to fall.

Figures 4, 5 shows the velocity and temperature of unsteady profiles oscillates with $M_1 = 1, M_2 = 2, K_1 = 0.1, K_2 = 0.23, k_1 = 1, k_2 = 0.5, Rd = 1, \omega = \pi/4, P_s = 2.5, P_o = 2, \alpha = 1, \beta = 2, \varepsilon_* = 0.1, Pr = 6.9, R = 0.02$. For plotting the graphs, the unsteady velocity and temperature distribution are taken as $u_t = \varepsilon e^{i\omega t}(u_{12} + u_{22})$ and $\theta_t = \varepsilon e^{i\omega t}(\theta_{12} + \theta_{22})$. From Fig. 4 the unsteady liquid of velocity profile shows oscillations with increasing frequency. Magnitude of the unsteady velocity is higher in region II. The unsteady temperature profile shows oscillations with a raise of ω that the magnitude of the unsteady temperature is higher in region I, of the oscillatory pressure gradient and the amplitude of the oscillations enhances with Ec , as shown in Fig. 5(c). Unsteady velocity and temperatures of cross-flow Reynolds numbers and magnetic field

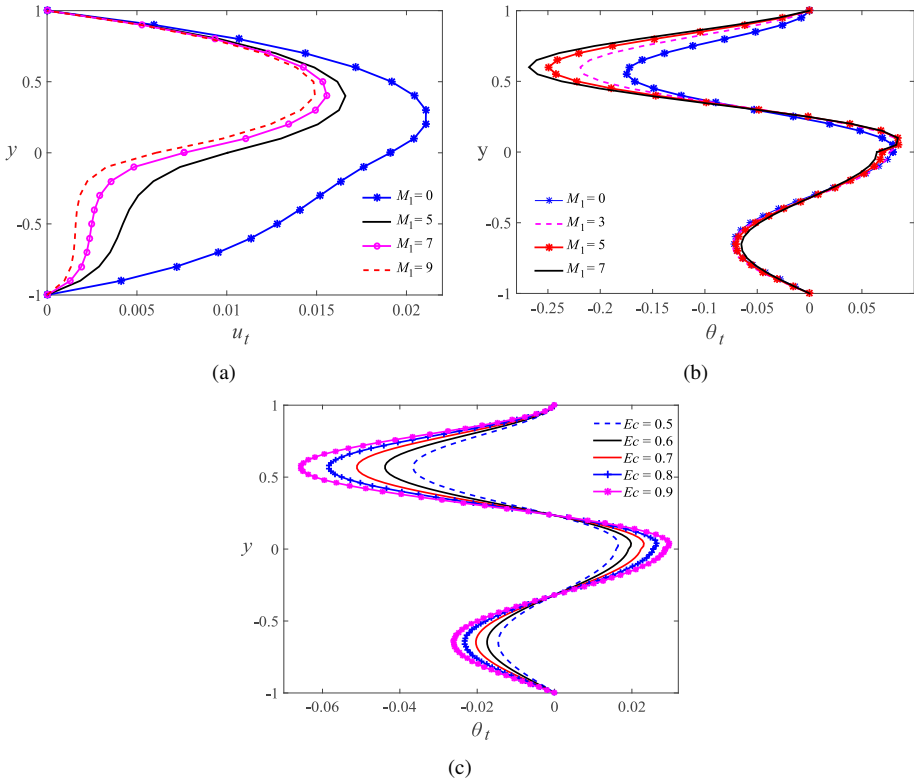


Figure 5. Variation of unsteady velocity and temperature profiles with (a)–(b) M_1 , (c) Ec .

are illustrated in Figs. 4(c), 4(d), 5(a), 5(b), respectively. In Fig. 4(c) the unsteady velocity in the lower region is higher than the upper region of the channel, and from Fig. 4(d) the unsteady temperature in the lower region will be higher and magnitude of the oscillations for the unsteady temperature distribution increases with R in region II and a reverse trend can be noticed in the other region. Further, maximum unsteady velocity occurs for hydrodynamic case (see Fig. 5(a)), and from Fig. 5(b) unsteady temperature will be greater for the hydrodynamic case with maximum deviations in the vicinity of the suction wall.

Figure 6 depicts the heat transfer rate at the walls of the channel for fixed values of $M_1 = 1, M_2 = 2, K_1 = 0.1, K_2 = 0.23, k_1 = 1, k_2 = 0.5, \omega = \pi/4, P_s = 2.5, P_o = 2, \alpha = 1, \beta = 1, R_1 = 1, \varepsilon_* = 0.1, Pr = 6.9, Ec = 0.5$. We can see from Figs. 6(a) and 6(b) that an increase in Eckert number enhances the rate of heat transfer at the injection wall, while it reduces at suction wall of the channel. Figures 6(c) and 6(d) indicates that as Rd increases, the heat transfer rate diminishes in the lower wall of the channel, while it raises at the suction wall.

For many relevant parameters, the analytical solution for shear stress is examined with $K_1 = 0.5, K_2 = 3, P_s = 2.5, P_o = 2, \omega t = \pi/8, \varepsilon_* = 0.1$, the results are shown in

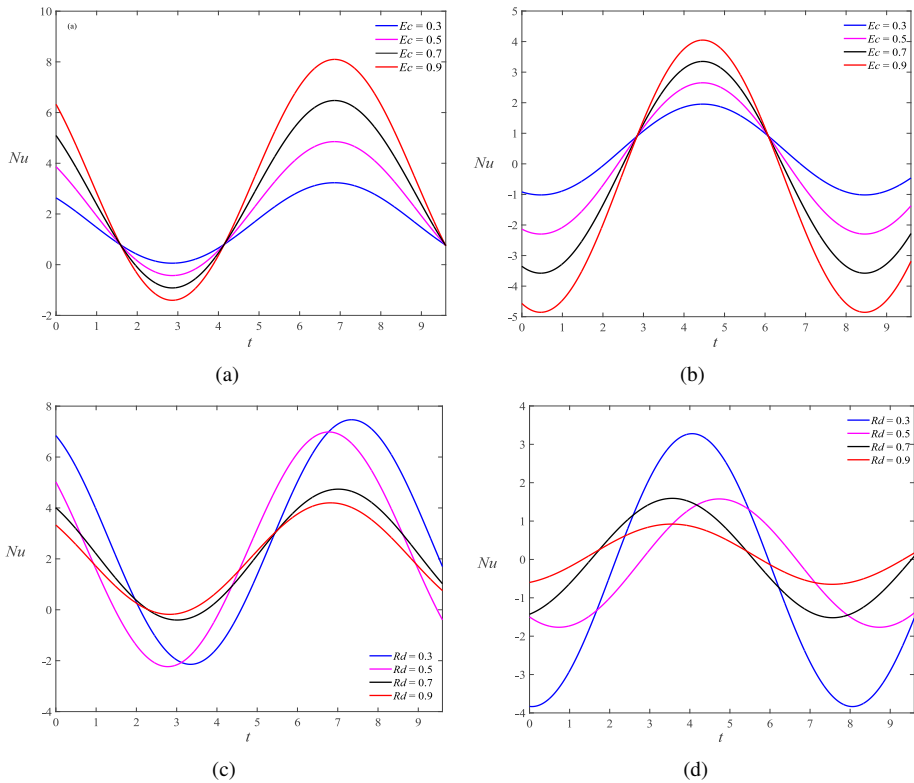


Figure 6. The effect of heat transfer rate at two walls with (a)–(b) Ec and (c)–(d) Rd

Tables 1–6. It has been observed from Tables 1, 2 that there is raise in viscosity, stress distribution at both the walls are higher at $\omega t = \pi/4, \pi/2, \pi$ and oscillates at $\omega t = 0$ in Table 1. At the lower wall of the channel the permeability raises, skin friction decreases at $\omega t = 0$ and oscillates with raise of $\omega t = \pi/4, \pi/2, \pi$ in Table 3. From Table 4 shear stress decreases with raise of ωt and oscillates at $\omega t = 0$. With a raise in ωt , skin friction at both walls falls from fixed values of other parameters. It is evident from Tables 5, 6 that the magnetic field strength raises, skin friction increases at $\omega t = \pi/4, \pi/2, \pi$ in Table 5 and $\omega t = 0$ in Table 6 and oscillates at $\omega t = 0$ in Table 5 and $\omega t = \pi/4, \pi/2, \pi$ in Table 6. Numerical values for mass flux are shown in Tables 7–9 for various physical parameters. It is observed that α and K_1 raise, mass flux increases (see Tables 7 and 8). Massflux has been evaluated for various values of M_1 , and the numerical values are shown in Table 9. It reveals that mass flux falls as the magnetic field strength raises with fixed values of other parameters. A comparative study with that of Umavathi et al. [28] is presented in Fig. 7(a). Further, the closed-form solutions obtained in the present study have been compared with the numerical values obtained by the Runge–Kutta method of the fourth-order coupled with the shooting approach solved in MATHEMATICA, and results have been depicted graphically in Figs. 7(b) and 7(c). It is found that the results are in good agreement.

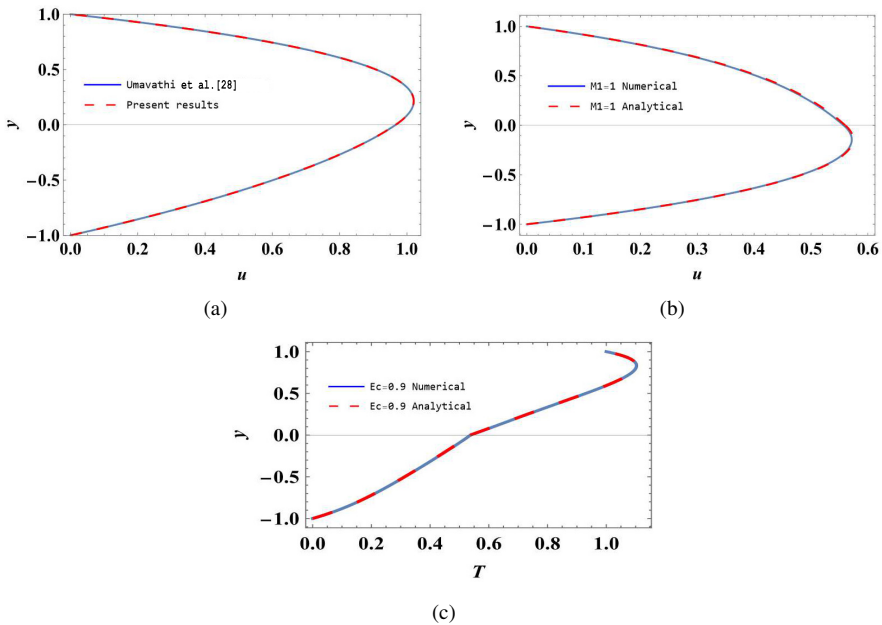


Figure 7. (a) Comparison of the results for velocity with previous and present paper with $M_1 = M_2 = M$, $K_1 = K_2 = 0$, $\rho_1 = \rho_2 = \rho_0$, $P_s = 2.5$, $P_o = 0$; (b)–(c) Comparison of the results for velocity and temperature observed analytically and numerically with $M_1 = 1$, $M_2 = 2$, $P_s = 2.5$, $P_o = 2$, $K_1 = 0.1$, $K_2 = 3$, $\alpha = 1$, $\beta = 1$.

6 Conclusions

This study was concerned with the oscillatory MHD two immiscible liquids flow in the porous space in a channel, with permeable boundaries. Thermal characteristics along with the thermal radiation have been accounted in the flow investigation. Solving the governing flow equations, closed-form solutions are obtained for physical variables of interest. The influence of pertinent parameters such as frequency, density ratio, viscosity ratio, the ratio of thermal conductivity, radiation, porosity, cross-flow Reynolds number, Hartmann number, Eckert number, and Prandtl number on flow variables have been studied. The results of these investigations could be helpful in the filtering process for various underground liquids, crude oil extraction, etc. The outcome of the important findings is summarized as follows.

- A rise in the magnitude of the oscillations in the unsteady velocity and temperature distributions occurs with the frequency parameter of the pressure gradient. The velocity of the fluid decreases with a rise in the frequency parameter and Hartmann number.
- A raise in the viscosity ratio parameter enhances the velocity of the fluid in both the regions and due to the decrease in the viscosity of the liquid, velocity will be higher in the region II of the channel when compared to the region I.

- As the permeability ratio of the porous media rises, the velocity distribution improves because barriers imposed on the flow channel decrease as P increases, allowing for free flow and therefore increasing velocity.
- Velocity distribution reduces in the lower region of the channel and enhances in the upper region with a rise in the cross-flow Reynolds number.
- As magnetic field strength increases the mass flux decreases.
- There is a fall in the temperature of the fluid with a raise in the crossflow Reynolds number.
- Temperature distribution enhances with a decrease in the thermal conductivity ratio, whereas increase in Eckert number, and Prandtl number.
- As the radiation raises, the heat transfer rate decreases at the lower boundary of the channel, and there will be a rise at upper boundary in the heat transfer rate.
- Rate of heat transfer falls as the radiation parameter rises at the lower wall and enhances at the upper wall of the channel.
- The results for the hydrodynamic problem can be obtained when $M_1, M_2 \rightarrow 0$. Further, the results of Umavathi et al. [28] can be recovered, as a limiting case, when $M_1 \rightarrow M, M_2 \rightarrow 0, K_1 \rightarrow 0, K_2 \rightarrow 0, \rho_1 = \rho_2 = \rho_0, Rd \rightarrow 0$ with constant pressure gradient for the corresponding problem.

References

1. S. Ahmed, A. Batin, A.J. Chamkha, Numerical/laplace transform analysis for mhd radiating heat/mass transport in a darcian porous regime bounded by an oscillating vertical surface, *Alex. Eng. J.*, **54**(1):45–54, 2015, <https://doi.org/10.1016/j.aej.2014.11.006>.
2. I.A. Ansari, S. Deo, Effect of magnetic field on the two immiscible viscous fluids flow in a channel filled with porous medium, *Natl Acad Sci Lett*, **40**(3):211–214, 2017, <https://doi.org/10.1007/s40009-017-0551-8>.
3. H.A. Attia, W. Abbas, M.A. Abdeen, M.S. Emam, Effect of porosity on the flow of a dusty fluid between parallel plates with heat transfer and uniform suction and injection, *Eur. J. Environ. Civ.*, **18**(2):241–251, 2014, <https://doi.org/10.1080/19648189.2013.860923>.
4. P. Bitla, F.Y. Sitotaw, Effects of slip and inclined magnetic field on the flow of immiscible fluids (couple stress fluid and jeffrey fluid) in a porous channel., *J. Appl. Math*, 2022, <https://doi.org/10.1155/2022/2799773>.
5. A.J. Chamkha, Non-darcy hydromagnetic free convection from a cone and a wedge in porous media, *Int. Commun. Heat Mass Transf.*, **23**(6):875–887, 1996, [https://doi.org/10.1016/0735-1933\(96\)00070-X](https://doi.org/10.1016/0735-1933(96)00070-X).
6. A.J. Chamkha, Mhd-free convection from a vertical plate embedded in a thermally stratified porous medium with hall effects, *Appl. Math. Model.*, **21**(10):603–609, 1997, [https://doi.org/10.1016/S0307-904X\(97\)00084-X](https://doi.org/10.1016/S0307-904X(97)00084-X).
7. A.J. Chamkha, Non-darcy fully developed mixed convection in a porous medium channel with heat generation/absorption and hydromagnetic effects, *Numer heat tr A-appl*, **32**(6):653–675, 1997, <https://doi.org/10.1080/10407789708913911>.

8. A.J. Chamkha, Flow of two-immiscible fluids in porous and nonporous channels, *J. Fluids Eng.*, **122**(1):117–124, 2000, <https://doi.org/10.1115/1.483233>.
9. A.J. Chamkha, J.C. Umavathi, A. Mateen, Oscillatory flow and heat transfer in two immiscible fluids, *International Journal of Fluid Mechanics Research*, **31**(1), 2004, <https://doi.org/10.1615/InterJFluidMechRes.v31.i1.20>.
10. M. Padma Devi, S. Srinivas, Thermal characteristics on two immiscible fluid flows in a porous space with time dependent pressure gradient, *Pp i mech eng e-j*, p. 09544089221096569, 2022, <https://doi.org/10.1177/09544089221096569>.
11. N.J. Hazarika, S. Ahmed, Thermo-diffusive flow of chemically reacting fluid in a saturated porous medium for radiative heat flux, *J. Sci. Res.*, **13**(2):507–520, 2021, <https://doi.org/10.3329/jsr.v13i2.50425>.
12. D.P. Hochmuth, D.K. Sunada, Ground-water model of two-phase immiscible flow in coarse material, *Groundw.*, **23**(5):617–626, 1985, <https://doi.org/10.1111/j.1745-6584.1985.tb01510.x>.
13. P. Bharath Kumar, S. Srinivas, Pulsating flow of a non-newtonian nanofluid in a porous channel with magnetic field, *Mater. Today: Proc.*, **9**:320–332, 2019, <https://doi.org/10.1016/j.matpr.2019.02.162>.
14. P.K. Mandal, An unsteady analysis of nonlinear two-layered 2d model of pulsatile flow through stenosed arteries, *Math. Model. Anal.*, **8**(3):229–246, 2003, <https://doi.org/10.1080/13926292.2003.9637226>.
15. S.K. Mishra, A.P. Verma, Imbibition in the flow of two immiscible fluids with magnetic field, *Phys. Fluids*, **17**(6):1338–1340, 1974, <https://doi.org/10.1063/1.1694889>.
16. B.A. Packham, R. Shall, Stratified laminar flow of two immiscible fluids, *Math. Proc. Camb. Philos. Soc.*, **69**(3):443–448, 1971, <https://doi.org/10.1017/S0305004100046880>.
17. J.D. Petrovic, Z.M. Stamenkkovic, M.M. Kocic, M.D. Nikodijevic-Dordevic, J.B. Bogdanovic-Jovanovic, D.D. Nikodijevic, Mhd flow and mixed convection of a viscous fluid and a nanofluid through a porous medium in a vertical channel, *Therm. Sci.*, pp. 188–188, 2022, <https://doi.org/10.2298/TSCI220903188P>.
18. O. Pouliquen, J.M. Chomaz, P. Huerre, Propagating holmboe waves at the interface between two immiscible fluids, *J. Fluid Mech.*, **266**:277–302, 1994, <https://doi.org/10.1017/S002211209400100X>.
19. G. Radhakrishnamacharya, M.K. Maiti, Heat transfer to pulsatile flow in a porous channel, *Int. J. Heat Mass Transf.*, **20**(2):171–173, 1977, [https://doi.org/10.1016/0017-9310\(77\)90009-6](https://doi.org/10.1016/0017-9310(77)90009-6).
20. A.R. Rao, S. Usha, Peristaltic transport of two immiscible viscous fluids in a circular tube, *J. Fluid Mech.*, **298**:271–285, 1995, <https://doi.org/10.1017/S0022112095003302>.
21. S. Ray, B. Unsal, F. Durst, Development length of sinusoidally pulsating laminar pipe flows in moderate and high reynolds number regimes, *Int J Heat Fluid Flow*, **37**:167–176, 2012, <https://doi.org/10.1016/j.ijheatfluidflow.2012.06.001>.
22. S. Srinivas, Ch. Kalyan Kumar, A. Subramanyam Reddy, Dufour and soret effects on pulsatile hydromagnetic flow of casson fluid in a vertical non-darcian porous space, *Nonlinear*

- Anal.: Model. Control*, **27**:1–15, 2022, <https://doi.org/10.15388/namc.2022.27.26678>.
23. A. Tiwari, S.S. Chauhan, Effect of varying viscosity on two-layer model of pulsatile flow through blood vessels with porous region near walls, *Transp Porous Media*, **129**(3):721–741, 2019, <https://doi.org/10.1007/s11242-019-01302-1>.
 24. J.C. Umavathi, O. Anwar Beg, Effects of thermophysical properties on heat transfer at the interface of two immiscible fluids in a vertical duct: numerical study, *Int. J. Heat Mass Transf.*, **154**:119613, 2020, <https://doi.org/https://doi.org/10.1016/j.ijheatmasstransfer.2020.119613>.
 25. J.C. Umavathi, A.J. Chamkha, A. Mateen, A. Al-Mudhaf, Unsteady two-fluid flow and heat transfer in a horizontal channel, *Heat Mass Transf.*, **42**(2):81–90, 2005, <https://doi.org/10.1007/s00231-004-0565-x>.
 26. J.C. Umavathi, A.J. Chamkha, A. Mateen, A. Al-Mudhaf, Unsteady oscillatory flow and heat transfer in a horizontal composite porous medium channel, *Nonlinear Anal.: Model.*, **14**(3):397–415, 2009, <https://doi.org/10.15388/NA.2009.14.3.14503>.
 27. J.C. Umavathi, I.C. Liu, J. Prathap Kumar, Magnetohydrodynamic poiseuille-couette flow and heat transfer in an inclined channel, *J. Mech.*, **26**(4):525–532, 2010, <https://doi.org/10.1017/S172771910000472X>.
 28. J.C. Umavathi, A. Mateen, A.J. Chamkha, A. Al-Mudhaf, Oscillatory hartmann two-fluid flow and heat transfer in a horizontal channel, *Int. J. Appl. Mech.*, **11**(1):155–178, 2006, <https://www.researchgate.net/publication/228899418>.
 29. M. VeeraKrishna, G. Subba Reddy, A.J. Chamkha, Hall effects on unsteady mhd oscillatory free convective flow of second grade fluid through porous medium between two vertical plates, *Phys. Fluids*, **30**(2):023106, 2018, <https://doi.org/10.1063/1.5010863>.
 30. A. Vijayalakshmi, S. Srinivas, A study on hydromagnetic pulsating flow of a nanofluid in a porous channel with thermal radiation, *J. Mech.*, **33**(2):213–224, 2017, <https://doi.org/https://doi.org/10.1017/jmech.2016.74>.
 31. C.Y. Wang, Starting flow in a channel with two immiscible fluids, *J. Fluids Eng.*, **139**(12), 2017, <https://doi.org/10.1115/1.4037495>.
 32. P.K. Yadav, A. Kumar, S. El-Sapa, A.J. Chamkha, Impact of thermal radiation and oriented magnetic field on the flow of two immiscible fluids through porous media with different porosity, *Waves Random Complex Media*, pp. 1–33, 2022, <https://doi.org/10.1080/17455030.2022.2118897>.
 33. A. Zaman, N. Ali, M. Sajid, T. Hayat, Numerical and analytical study of two-layered unsteady blood flow through catheterized artery, *PLoS One*, **11**(8):e0161377, 2016, <https://doi.org/10.1371/journal.pone.0161377>.